



Nonlinear generation of Airy vortex beam

HUI LI,^{1,2} HAIGANG LIU,^{1,2} AND XIANFENG CHEN^{1,2,*}

¹ State Key Laboratory of Advanced Optical Communication Systems and Networks, School of Physics and Astronomy, Shanghai Jiao Tong University, Shanghai 200240, China

² Key Laboratory for Laser plasma (Ministry of Education), Collaborative Innovation Center of IFSA (CICIFSA), Shanghai Jiao Tong University, Shanghai 200240, China

*xfchen@sjtu.edu.cn

Abstract: Recently, hybrid beams have sparked considerable interest because of their properties coming from different kinds of beams at the same time. Here, we experimentally demonstrate Airy vortex beam generation in the nonlinear frequency conversion process when the fundamental wave with its phase modulated by a spatial light modulator is incident into a homogeneous nonlinear medium. In our experiments, second harmonic Airy circle vortex beams and Airy ellipse vortex beams were generated and the topological charge was also measured. The parabolic trajectory of those Airy vortex beams can be easily adjusted by altering the fundamental wave phase. This study provides a simple way to generate second harmonic Airy vortex beams, which may broaden its future use in optical manipulation and light-sheet microscopy.

© 2018 Optical Society of America under the terms of the [OSA Open Access Publishing Agreement](#)

1. Introduction

The first observation of the optical orbital angular momentum (OAM) could go back to 1936 [1]. It was until 1992 that Allen et al. verified that optical OAM has an azimuthal phase term $e^{il\varphi}$, where l represents the topological charge and φ is the azimuth angle [2]. The discovery of the optical OAM incubated an avenue of potential applications in various research fields, such as optical trapping [3–7], quantum computation [8], and optical communications [9]. It is worth noting that a considerable attention has also been paid to some new kinds of beams for their special properties [2,10–17]. So far, optical vortex beam has been reported combined with other types of beams, such as Laguerre–Gaussian (LG) vortex beam [2], Bessel vortex beam [10]. Besides, the research on the propagation of an OAM implanted onto Airy beam, which is called Airy vortex beam (AVB), sparked considerable interest [11–17]. The Airy packet as a solution of the Schrödinger equation was first proposed by Berry and Balazs in 1979 [18]. Since the first observation in optics, Airy beam has been a subject of great interest for its self-acceleration [19], self-healing [20] and non-diffraction [21] properties during propagation as well as its further application in optical manipulation [22], light-sheet microscopy [23], etc. In AVB, vortex beam has the ability of propagating along a curved parabolic trajectory under the impact of the Airy beam [12,13]. The properties of various types of AVB have been investigated in simulated environment [12,24,25]. In terms of experimental realization, there are two main methods to get the AVB. One method is to fabricate the crystal into specific pattern [11,14,17]. Nevertheless, the fabrication process is time consuming and the desired metasurface always generate fixed wave pattern. In this method, it is difficult to ensure the main lobe of the Airy beam and the center of the vortex phase are in alignment. The other way is to introduce the optical vortex beam to a cubic phase or a 3/2 phase profile [13,16]. Until now, such AVB is only realized in the linear process [11–15].

In this paper, we experimentally demonstrated a simple method to generate the nonlinear AVB by controlling the fundamental wave (FW) phase manipulation by a spatial light modulator (SLM). The nonlinear process enables AVB obtained at a new wavelength. The result shows that the main lobe of the Airy beam splits into two parts. With the increasing of absolute value of the topological charge, the gap between two parts becomes larger. The

dislocation of such AVB moves aside when vortex part changes from circle to ellipse. In both cases, the topological charge of the SH AVB is measured. Besides, we theoretically calculated and experimentally measured the relationship between the AVB deflection and propagation distance.

2. Theoretical analysis

Supposing the light propagates along the z-axis, the FW can be written as:

$$E_1 = A_1 \exp[-i(k_1 z - \omega t)] \cdot \exp\left[i\left(\frac{x^3}{d^3} + \frac{y^3}{d^3}\right) + il_1 \varphi\right], \quad (1)$$

where A_1 and k_1 are the amplitude and wave vector of the FW, respectively. $\exp\left[i\left(\frac{x^3}{d^3} + \frac{y^3}{d^3}\right)\right]$ is the cubic phase term, d represents the transverse scale of Airy beam. l_1 is the OAM of FW, $\varphi = \tan^{-1}(y/x)$ is the azimuthal angle. We consider the SH wave expressed as $E_2 = A_2 \exp[-i(k_{2z} z - 2\omega t)]$, where A_2 and k_{2z} represent the amplitude and longitudinal wavevector of the SH beam, respectively. Under the undepleted-pump and paraxial approximation, we have an equation that describes the SHG light field as:

$$\frac{dA_2}{dz} = \varepsilon_0 \chi^{(2)} A_1^2 \cdot \exp[i(k_{2z} - 2k_1)z] \cdot \exp\left[2i\left(\frac{x^3}{d^3} + \frac{y^3}{d^3}\right)\right] \cdot \exp(2il_1 \varphi). \quad (2)$$

In this case, we can deduce that the left exponent term is the phase mismatch of the nonlinear process, and the following exponential terms stand for the SH Airy beam and the topological charge of SH vortex beam, respectively. In our experiment, the FW propagates along the birefringent phase matching direction. The wavevectors of the second harmonic and fundamental waves satisfy a momentum conservation law, $k_{2z} - 2k_1 = 0$. Thus, the amplitude at the exit plane of the nonlinear medium is given:

$$A_2 = \varepsilon_0 \chi^{(2)} A_1^2 L \cdot \exp\left[2i\left(\frac{x^3}{d^3} + \frac{y^3}{d^3}\right)\right] \cdot \exp(2il_1 \varphi). \quad (3)$$

L is the thickness of the nonlinear crystal. In this case, SHG with a cubic phase emerges from the transverse component of the FW. The topological charge of the generated SH wave can be expressed as: $l_{SH} = 2l_1$, where l_{SH} is the topological charge of the SH wave. The SH AVB obtains after an optical Fourier transform of Eq. (3) [19]. It is clearly that AVB can be generated from modulated FW rather than desired crystal into fixed pattern.

3. Experimental results and discussion

The experimental setup is depicted in Fig. 1. In our experiment, a Nd:YAG Q-switched laser with a wavelength of 1064 nm is used to emit a Gaussian beam. The duration and repetition rate of the laser pulses are ~4 ns and 20 Hz, respectively. A half wave plate (HWP) and a Glan-Taylor (GT) prism are used to control intensity and polarization of the FW. The laser beam is subsequently expanded and collimated (L1 and L2) before incidents onto the SLM, after which the modulated FW passes through a 4-f system (consisting of L3 and L4) and projects onto the sample. After the 4-f system, the beam waist of the phase modulated FW is approximately 0.14 mm as shown in the inset of Fig. 1(a). A NIR detector card is used to convert the FW at 1064 nm to visible red light. The sample is a homogenous 5-mol% MgO:LiNbO₃ crystal ($10 \times 10 \times 0.5$ mm³ in $x \times y \times z$ dimensions). The angle between propagation direction (z-axis) and optic axis of the crystal is 75° according to the Sellmeier

equation in [26]. The reflective phase only SLM (Holoeye Pluto) has a resolution of 1920×1080 pixels and the pixel pitch is $8 \mu\text{m}$. Lens L5 with focal length of 50 mm is used to perform the Fourier transformation. A filter (F) is placed after the crystal to obstruct the FW and maintain the SH wave. At last, the SH AVB is imaged on a screen and recorded by a camera.

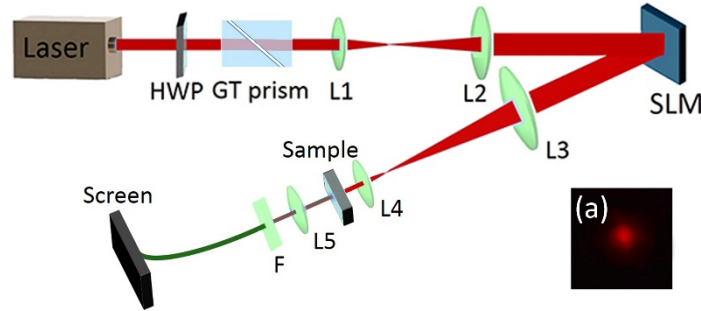


Fig. 1. Schematic of the experimental setup. Inset (a) shows the FW before the sample. The following denotations are used: HWP, half wave plate; GT prism, Glan-Taylor prism; L1,...,5, lens; focal length L1,...,5 = 50, 100, 200, 30, and 50 mm, respectively; Sample, 5-mol% MgO:LiNbO₃; F, filter.

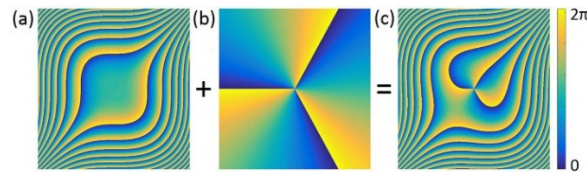


Fig. 2. Generation of the phase mask. (a) Cubic phase, (b) Spiral phase with topological charge $l_1 = 3$, (c) Airy vortex phase mask.

The generation process of the phase mask is shown in Fig. 2. Here, we define the phase mask according to the equation $T = \exp\left[i\left(\frac{x^3}{d^3} + \frac{y^3}{d^3}\right) + il_1\varphi\right]$, where $d = 0.48\text{mm}$. This phase mask can be generated by adding the spiral phase pattern on a cubic phase mask, which is modulated in the range of 0 to 2π . Figure 2(a) is the cubic phase mask and Fig. 2(b) depicts a spiral phase with topological charge $l_1 = 3$. Finally, the phase mask shown in Fig. 2(c) is loaded on the SLM.

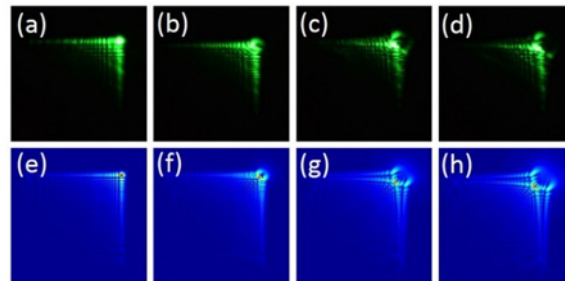


Fig. 3. The experiment (a)–(d) and simulation (e)–(h) results of the SH AVBs with topological charge $l_{SH} = 0, 2, 6, 8$, respectively.

We demonstrate the generation of SH AVBs with different topological charge shown in Fig. 3. Figures 3(a)–3(d) represent the experimentally generated AVBs with topological charge $l_{SH} = 0, 2, 6, 8$, which are close to the theoretical calculated results shown in Figs. 3(e)–3(h). The simulation results display in the bottom row of Fig. 3 is based on Eq. (3). Compared to the SH Airy beam of Fig. 3(a), SH AVBs have a dislocation in the center main lobe which makes it split into two parts as shown in Figs. 3(b), 3(c), and 3(d). As we know, the radius of the vortex beam got larger as the topological charge increased [27]. In our experiment, with the increasing of the topological charge, the gap between two parts gets larger as well.

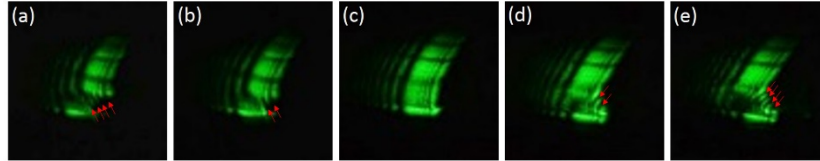


Fig. 4. The measurement of the topological charge by a cylindrical lens with $l_{SH} = -4, -2, 0, 2, 4$, respectively.

The topological charge of the SH AVB is measured by a cylindrical lens shown in Fig. 4 [16,28], where the intensity of the astigmatic AVB is influenced by the topological charge. The astigmatic transformation of Airy beam stretches the lobe along the vertical direction, as shown in Fig. 4(c). It is noteworthy that Figs. 4(a), 4(b), 4(d), and 4(e) have some dark stripes in contrast with Fig. 4(c). As depicted in Figs. 4(a) and 4(b), part of the bright stripes disappear due to the interference between the astigmatic Airy beam and vortex beam as the dark stripes of the astigmatic vortex beam tilted to the left. As for the topological charge is positive, shown in Figs. 4(d) and 4(e), dark stripes in front of the main part of the astigmatic Airy beam tilt to the right. For clarity, arrows shown in Fig. 4 mark the number and orientation of dark stripes. From the number and orientation of dark stripes, we can arrive at the topological charge of the SH AVB.

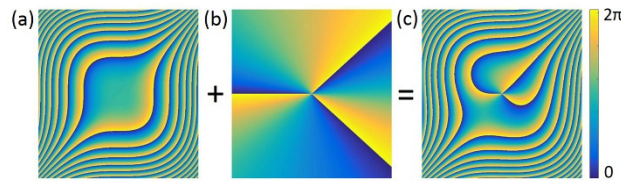


Fig. 5. Generation of the phase mask. (a) Cubic phase, (b) a asymmetric spiral phase with topological charge $l = 3$, $a = 2$, (c) Airy ellipse vortex phase mask.

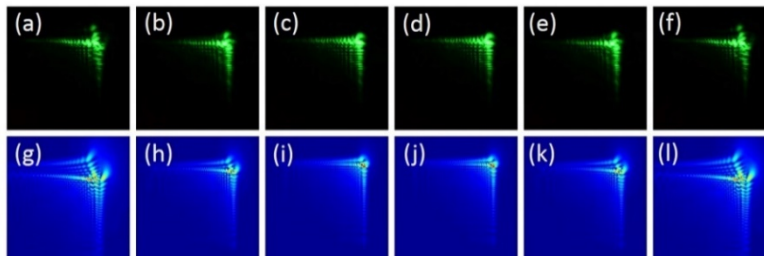


Fig. 6. The experiment (a)–(f) and simulation (g)–(l) results of the generated SH AVBs with topological charge $l_{SH} = -8, -4, -2, 2, 4, 8$, respectively.

Similarly, we also consider the generation of Airy ellipse vortex beam, in which the azimuthal angle changes according to $\varphi = \tan^{-1}(ay/x)$, take for $a = 2$ as an example. The final phase mask is displayed in Fig. 5(c) and the phase changes continuously from 0 to 2π as well. Figure 5(a) denotes the cubic phase mask. In this case, the spiral phase shown in Fig. 5(b) is asymmetric. The experiment and simulation results are displayed in the first and second rows of Fig. 6, respectively. As expected, the gap becomes larger as the topological charge increases. Different with Fig. 3, the dislocation moves up due to OAM density mainly concentrated on the small side of the ellipse [29]. As a result, it brings more possibility application with adjustable eccentricity of the ellipse. We measure the topological charge in the same way and the result is consistent with the theory $l_{SH} = 2l_1$.

In addition, the parabolic trajectory of the SH AVB vividly describes deflection along the propagation distance and is calculated according to the expression $y \cong \lambda^2 z^2 / (16\pi^2 d_0^3)$ [12,19], where λ is the wavelength of SH beam, and d_0 is approximately $54\mu\text{m}$ as a result of 4f-system and nonlinear process. In Fig. 7, the solid line stands for the analytic solution while circles correspond to the experiment results. The images of SH AVBs at different propagation distance are provided as insets. The evolution of deflection is clearly to see. In this way, it is possible to adjust the deflection just by dynamically changing the phase of the fundamental beam.

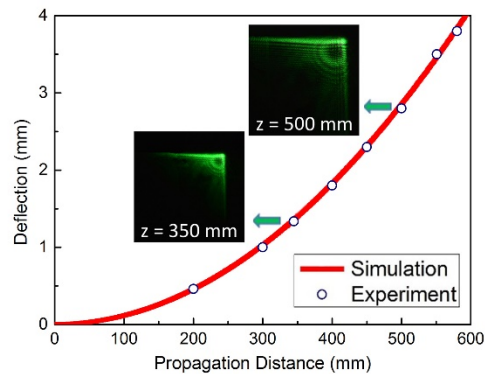


Fig. 7. Transverse acceleration of an AVB as a function of distance. The solid line is the analytic solution and circles correspond to the experimental results. The images of SH AVBs at different propagation distance are provided as insets.

The method proposed in this paper has the ability of dynamic and programmable modulation of SH AVB. Using this method, it is possible to generate other nonlinear hybrid beams in a straightforward way. Besides, more nonlinear processes such as up-conversion and down-conversion processes can also be studied.

4. Conclusion

In summary, we have experimentally demonstrated the generation of nonlinear AVB by modulating the phase of the FW, which incidents into a homogeneous nonlinear crystal. Both Airy circle vortex beam and Airy ellipse vortex beam are investigated in experimental and simulated environment. The experiment and simulation results are coincident. The topological charge of SH AVB is measured, which is the same to the analysis. Moreover, the relationship between parabolic trajectory and transverse scale d_0 is considered. This study provides a simple way to dynamically generate SH AVB which may have further application in optical manipulation, light-sheet microscopy, and so on.

Funding

National Key R&D Program of China (2017YFA0303700); National Natural Science Foundation of China (NSFC) (11734011); The Foundation for Development of Science and Technology of Shanghai (17JC1400400).

References

1. R. A. Beth, "Mechanical detection and measurement of the angular momentum of light," *Phys. Rev.* **50**(2), 115–125 (1936).
2. L. Allen, M. W. Beijersbergen, R. J. C. Spreeuw, and J. P. Woerdman, "Orbital angular momentum of light and the transformation of Laguerre-Gaussian laser modes," *Phys. Rev. A* **45**(11), 8185–8189 (1992).
3. D. G. Grier, "A revolution in optical manipulation," *Nature* **424**(6950), 810–816 (2003).
4. M. F. Andersen, C. Ryu, P. Cladé, V. Natarajan, A. Vaziri, K. Helmerson, and W. D. Phillips, "Quantized rotation of atoms from photons with orbital angular momentum," *Phys. Rev. Lett.* **97**(17), 170406 (2006).
5. M. Padgett and R. Bowman, "Tweezers with a twist," *Nat. Photonics* **5**(6), 343–348 (2011).
6. J. E. Curtis and D. G. Grier, "Structure of optical vortices," *Phys. Rev. Lett.* **90**(13), 133901 (2003).
7. Z. Shen, L. Su, X. C. Yuan, and Y. C. Shen, "Trapping and rotating of a metallic particle trimer with optical vortex," *Appl. Phys. Lett.* **109**(24), 241901 (2016).
8. A. Mair, A. Vaziri, G. Weihs, and A. Zeilinger, "Entanglement of the orbital angular momentum states of photons," *Nature* **412**(6844), 313–316 (2001).
9. J. Wang, J. Y. Yang, I. M. Fazal, N. Ahmed, Y. Yan, H. Huang, Y. Ren, Y. Yue, S. Dolinar, M. Tur, and A. E. Willner, "Terabit free-space data transmission employing orbital angular momentum multiplexing," *Nat. Photonics* **6**(7), 488–496 (2012).
10. F. G. Mitri, "Vector wave analysis of an electromagnetic high-order Bessel vortex beam of fractional type α ," *Opt. Lett.* **36**(5), 606–608 (2011).
11. B. Wei, S. Liu, P. Chen, S. Qi, Y. Zhang, W. Hu, Y. Lu, and J. Zhao, "Vortex Airy beams directly generated via liquid crystal q-Airy-plates," *Appl. Phys. Lett.* **112**(12), 121101 (2018).
12. H. T. Dai, Y. J. Liu, D. Luo, and X. W. Sun, "Propagation dynamics of an optical vortex imposed on an Airy beam," *Opt. Lett.* **35**(23), 4075–4077 (2010).
13. H. T. Dai, Y. J. Liu, D. Luo, and X. W. Sun, "Propagation properties of an optical vortex carried by an Airy beam: experimental implementation," *Opt. Lett.* **36**(9), 1617–1619 (2011).
14. J. Zhou, Y. Liu, Y. Ke, H. Luo, and S. Wen, "Generation of Airy vortex and Airy vector beams based on the modulation of dynamic and geometric phases," *Opt. Lett.* **40**(13), 3193–3196 (2015).
15. R. Shiloh, Y. Tsur, R. Remez, Y. Lereah, B. A. Malomed, V. Shvedov, C. Hnatovsky, W. Krolikowski, and A. Arie, "Unveiling the Orbital Angular Momentum and Acceleration of Electron Beams," *Phys. Rev. Lett.* **114**(9), 096102 (2015).
16. B. K. Singh, R. Remez, Y. Tsur, and A. Arie, "Measurement of acceleration and orbital angular momentum of Airy beam and Airy-vortex beam by astigmatic transformation," *Opt. Lett.* **40**(22), 5411–5414 (2015).
17. B. Wei, P. Chen, S. Ge, W. Duan, W. Hu, and Y. Lu, "Generation of self-healing and transverse accelerating optical vortices," *Appl. Phys. Lett.* **109**(12), 121105 (2016).
18. M. V. Berry and N. L. Balazs, "Nonspreading wave packets," *Am. J. Phys.* **47**(3), 264–267 (1979).
19. G. A. Siviloglou, J. Broky, A. Dogariu, and D. N. Christodoulides, "Observation of Accelerating Airy Beams," *Phys. Rev. Lett.* **99**(21), 213901 (2007).
20. J. Broky, G. A. Siviloglou, A. Dogariu, and D. N. Christodoulides, "Self-healing properties of optical Airy beams," *Opt. Express* **16**(17), 12880–12891 (2008).
21. X. H. Hong, B. Yang, C. Zhang, Y. Q. Qin, and Y. Y. Zhu, "Nonlinear volume holography for wave-front engineering," *Phys. Rev. Lett.* **113**(16), 163902 (2014).
22. J. Baumgartl, M. Mazilu, and K. Dholakia, "Optically mediated particle clearing using Airy wavepackets," *Nat. Photonics* **2**(11), 675–678 (2008).
23. T. Vettenburg, H. I. Dalgarno, J. Nylk, C. Coll-Lladó, D. E. Ferrier, T. Čížmár, F. J. Gunn-Moore, and K. Dholakia, "Light-sheet microscopy using an Airy beam," *Nat. Methods* **11**(5), 541–544 (2014).
24. Y. Jiang, K. Huang, and X. Lu, "Propagation dynamics of abruptly autofocusing Airy beams with optical vortices," *Opt. Express* **20**(17), 18579–18584 (2012).
25. J. Zhuang, D. Deng, X. Chen, F. Zhao, X. Peng, D. Li, and L. Zhang, "Spatiotemporal sharply autofocused dual-Airy-ring Airy Gaussian vortex wave packets," *Opt. Lett.* **43**(2), 222–225 (2018).
26. O. Gayer, Z. Sacks, E. Galun, and A. Arie, "Temperature and wavelength dependent refractive index equations for MgO-doped congruent and stoichiometric LiNbO₃," *Appl. Phys. B* **91**(2), 343–348 (2008).
27. N. V. Bloch, K. Shemer, A. Shapira, R. Shiloh, I. Juviler, and A. Arie, "Twisting light by nonlinear photonic crystals," *Phys. Rev. Lett.* **108**(23), 233902 (2012).
28. V. Denisenko, V. Shvedov, A. S. Desyatnikov, D. N. Neshev, W. Krolikowski, A. Volyar, M. Soskin, and Y. S. Kivshar, "Determination of topological charges of polychromatic optical vortices," *Opt. Express* **17**(26), 23374–23379 (2009).
29. A. A. Kovalev, V. V. Kotlyar, and A. P. Porfirev, "A highly efficient element for generating elliptic perfect optical vortices," *Appl. Phys. Lett.* **110**(26), 261102 (2017).